JOURNAL OF GEOPHYSICAL RESEARCH, VOL. 94, NO. C1, PAGES 951–966, JANUARY 15, 1989

Wave Transformation and Swash Oscillation on Gentle and Steep Slopes

NOBUHISA KOBAYASHI AND GUNAMUNI S. DESILVA

Ocean Engineering Program, Department of Civil Engineering, University of Delaware, Newark

KEITH D. WATSON

U.S. Army Corps of Engineers, Philadelphia District, Pennsylvania

The numerical model developed previously for coastal structures is slightly modified and applied to predict the wave transformation in the surf and swash zones on gentle slopes as well as the wave reflection and swash oscillation on relatively steep beaches. The numerical model is one-dimensional in the cross-shore direction and is based on the finite amplitude, shallow water equations, including the effect of bottom friction, which are solved in the time domain for the incident wave train specified as input at the seaward boundary of the computation located outside the breakpoint. The slight modification is related to the effect of the time-averaged current on the seaward boundary condition and improves the agreement between the computed and measured mean water levels on gentle slopes. The modified numerical model is compared with available small-scale test data for monochromatic waves spilling on gentle slopes as well as for monochromatic waves plunging and surging on a relatively steep slope. Additional comparisons are made with small-scale tests conducted using transient monochromatic and grouped waves on a 1:8 smooth slope with and without an idealized nearshore bar at the toe of the 1:8 slope. As a whole, the numerical model is shown to be capable of predicting both time-varying and time-averaged hydrodynamic quantities in the surf and swash zones on gentle as well as steep slopes.

INTRODUCTION

Analyses of the transformation of incident wind waves on a gently sloping beach generally assume that the incident wave energy is dissipated completely in a wide surf zone and that no wave reflection occurs from the beach face. The idealization of inviscid, initially irrotational, flow has been proved to be sufficiently successful for predicting when and how waves break [*Peregrine*, 1983]. At present there is no rigorous model available for predicting the flow characteristics immediately after wave breaking. After the rapid transitions in the outer surf zone, breaking waves settle into the quasi steady state in which the wave form changes relatively slowly and has a strongly turbulent region on the face of the wave, called a surface roller [*Svendsen et al.*, 1978]. The broken waves in the inner surf zone hence resemble bores. For normally incident waves on a long straight beach of gentle slope the one-dimensional time-averaged equations of energy and momentum were applied to predict the variations of wave height and setup across the surf zone for monochromatic waves [e.g., *Svendsen*, 1984*a*] as well as for random waves [e.g., *Battjes and Stive*, 1985]. These quasi-steady models based on the assumption of borelike waves were shown to be sufficiently accurate except that the mean water level in the outer surf zone was predicted to rise too far seaward. Furthermore, the vertical variations of the time-averaged momentum and mass balances were analyzed to predict the vertical distribution of the time-averaged current (undertow) flowing seaward below the wave trough in the surf zone [e.g., *Svendsen et al.*, 1987]. In addition to the time-averaged quantities such as the undertow and setup, knowledge of the time-varying quantities such as the oscillatory velocities and swash oscillation is required for predicting the cross-shore sediment transport using a sediment transport model such as the relatively simple model of *Bailard* [1981] which expresses the instantaneous rate of total load (bed load plus suspended load) as a function of the instantaneous near-bottom water velocity and the local bed slope. The analyses of *Guza and Thornton* [1985*a*] and *Stive* [1986] based on the Bailard's model indicated that asymmetries in the oscillatory wave field and the interaction of the undertow with the wave field would produce the net onshore and offshore sediment transport in the surf zone, respectively. However, the velocity asymmetry associated with the wave profile asymmetry about the vertical axis cannot be predicted by existing wave theories such as Stokes and cnoidal wave theories [*Flick et al.*, 1981]. In order to predict the time-varying behavior of bores across the surf and swash zones on a beach, *Hibberd and Peregrine* [1979] and *Packwood* [1980] solved the finite amplitude, shallow water equations numerically in the time domain. *Svendsen and Madsen* [1984] included the effects of turbulence generated by wave breaking to describe a turbulent bore in the surf zone only.

In terms of the measured swash oscillations [e.g., *Guza and Thornton*, 1982] as well as the measured cross-shore velocity variances [e.g., *Guza and Thornton*, 1985*a*] field observations on gently sloping beaches have indicated that low-frequency (surf beat) motions in the period range that is greater than that associated with the incident wind waves may become dominant near the shoreline. A recent review of coastal processes and shoreline erosion by *Komar and Holman* [1986] emphasized the importance of the low-frequency motions. These low-frequency motions may be in the form of edge waves [e.g., *Oltman-Shay and Guza*, 1987] and standing waves in the cross-shore direction [e.g., *Guza and Thornton*, 1985*b*]. At present the low-frequency motions are not predictable for given incident wind waves and beach geometry. *Symonds et al.* [1982] proposed a one-dimensional model for long wave generation by the temporal variation of the wave setup which was assumed to respond instantaneously to the time-varying breakpoint of normally incident wave groups. This model was

Paper number 88JC03535.
0148-0227/89/88JC-03535$05.00

extended by *Symonds and Bowen* [1984] to include a linear shore-parallel bar. The modeling of the wave setup in these models may not be very accurate in light of the data and analysis presented by *Stive and Wind* [1982] as well as the transient shoreline response computed in this paper.

For steep beaches the incident wind waves may break on the foreshore as plunging or collapsing breakers or surge up on the foreshore with little wave breaking [e.g., *Battjes*, 1974; *Peregrine*, 1983]. The inner surf zone characterized by the quasi steady state does not exist on a steep beach. Reflection of the incident wave energy from the steep foreshore may not be negligible even for plunging breakers. Standing wave solutions based on the shallow water equations may be used for surging waves [e.g., *Suhayda*, 1974; *Guza and Bowen*, 1976], but no theoretical model except for those based on the assumption of potential flow [e.g., *New et al.*, 1985] is available for predicting the turbulent unsteady flow characteristics resulting from plunging and collapsing breakers. Moreover, subharmonic edge waves may be generated and grow for the case of surging waves [e.g., *Guza and Bowen*, 1976].

A specific beach with given geometry, which tends to be concave upward, may be dissipative or reflective depending on the incident wave characteristics and the tide and storm surge levels, as implied from the extensive field measurements of wave setup and swash on a moderately steep beach made by *Holman and Sallenger* [1985]. Consequently, it is desirable to develop a single model which can predict both time-varying and time-averaged hydrodynamic quantities in the surf and swash zones on a beach of arbitrary geometry and reflectance, although such a model may require significant computational efforts. Numerical models based on the Boussinesq equations for a sloping bottom [*Peregrine*, 1967] were already developed and applied for predicting the wave transformation outside the surf zone. *Abbott et al.* [1978, 1984] solved the two-dimensional Boussinesq equations in the time domain. Their numerical model was verified against analytical and experimental results for shoaling, refraction, diffraction, and partial reflection processes [*Madsen and Warren*, 1984]. On the other hand, *Freilich and Guza* [1984] developed a frequency domain model based on the one-dimensional Boussinesq equations to predict the nonlinear evolution of the wave field's Fourier amplitudes and phases. *Elgar and Guza* [1985*a*, 1985*b*, 1986] showed utility of the frequency domain model coupled with bispectral techniques for predicting and analyzing the observed nonlinear evolution of shoaling random waves.

In this paper the numerical model of *Kobayashi et al.* [1987] that was developed for coastal structures whose slopes are steeper than steep beaches is slightly modified and applied to predict the time-varying and time-averaged hydrodynamic quantities in the surf and swash zones on beaches of gentle and steep slopes. *Kobayashi et al.* [1987] modified the numerical model based on the one-dimensional finite amplitude, shallow water equations developed for beaches by *Hibberd and Peregrine* [1979] and *Packwood* [1980] in order to predict the uprush and downrush of normally incident monochromatic waves on the rough impermeable slope of a coastal structure. The modified numerical model was shown to yield good agreement with available large-scale and small-scale test data on the maximum runup and reflection of monochromatic waves plunging, collapsing, and surging on uniform and composite riprap slopes. *Kobayashi and Greenwald* [1986, 1988] conducted small-scale tests using a 1:3 gravel slope with an impermeable base to further calibrate and evaluate the numerical model. The calibrated numerical model was shown to be capable of predicting the measured temporal variations of the hydrodynamic quantities on the rough impermeable slope. Moreover, *Kobayashi and Watson* [1987] showed that the numerical model could also be applied to coastal structures with smooth slopes by adjusting the friction factor associated with the slope roughness. These comparisons were limited to monochromatic waves on slopes of 1:5 or steeper. It is hence not obvious whether this numerical model can be applied to beaches of gentler slopes, although the original model of *Hibberd and Peregrine* [1979] and *Packwood* [1980] produced the results which appeared realistic and promising. The numerical model used in this paper is one-dimensional in the cross-shore direction and cannot deal with edge waves. The normally incident wave train, specified as input at the seaward boundary of the numerical computation performed in the time domain, can be irregular as well as monochromatic, but the time domain computation is not efficient for the incident irregular wave train of long duration, which needs to be specified as input for the simulation of low-frequency motions in the cross-shore direction. As a result, the present computations are limited to incident monochromatic and transient grouped wave trains. Furthermore, this numerical model predicts the instantaneous depth-averaged horizontal velocity only and cannot predict the vertical velocity variations. In spite of this limitation the numerical model is shown to predict the time-averaged horizontal velocity directed in the seaward direction, although the predicted time-averaged velocity is found to be smaller than the undertow velocity measured below the wave trough.

In the following the numerical model of *Kobayashi et al.* [1987] with a slight modification of the seaward boundary condition is presented concisely. The slight modification is related to the effect of the time-averaged current on the seaward boundary condition and improves the agreement between the computed and measured mean water levels on gentle slopes. The modified numerical model is compared with small-scale test data for monochromatic waves spilling on gentle slopes. The comparison includes the comprehensive test results for a 1:40 slope presented by *Stive* [1980] and *Stive and Wind* [1982] as well as the undertow measurement for a 1:34.25 slope performed by *Hansen and Svendsen* [1984]. The numerical model is shown to be capable of predicting the development of the wave profile asymmetry about the vertical axis from the symmetric cnoidal wave profile outside the breakpoint to the sawtooth profile in the inner surf zone. The computed shoreline oscillation on the gentle slope shows the dominance of the setup over the swash in accordance with the saturation hypothesis proposed by *Huntley et al.* [1977]. The numerical model is also compared with the wave reflection and swash excursion measurements for monochromatic waves plunging and surging on a 1:8.14 slope described by *Guza and Bowen* [1976] and *Guza et al.* [1984]. In addition, small-scale tests were conducted to evaluate the capability of the numerical model for predicting the measured temporal variations of the reflected wave train and the shoreline oscillation on a relatively steep beach. The tests included three runs for monochromatic waves on a 1:8 slope, three runs for transient grouped waves on a 1:8 slope, and three runs for monochromatic waves on a 1:8 slope with an idealized bar at the toe of the 1:8 slope. As a whole, the numerical model is shown to be applicable to both gentle and steep beaches.

ONE-DIMENSIONAL UNSTEADY NUMERICAL MODEL

Kobayashi et al. [1987] solved the finite amplitude, shallow water equations for arbitrary slope geometry numerically in

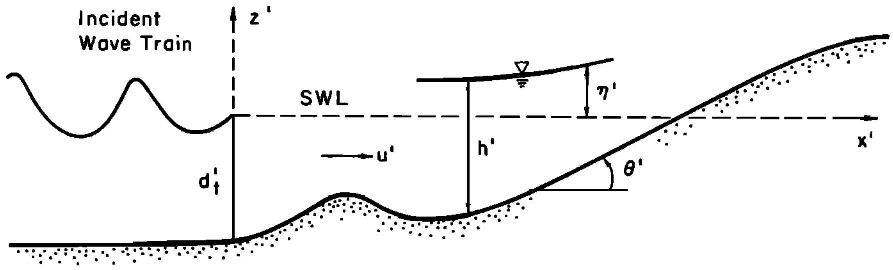

Fig. 1. Definition sketch for numerical model.

the time domain. The two-dimensional coordinate system (x', z') used in this paper is defined in Figure 1 in which the prime indicates the physical variables. The x' coordinate is taken to be positive in the landward direction with $x' = 0$ at the seaward boundary where the incident wave train is specified as input. The z' coordinate is taken to be positive upward with $z' = 0$ at the still water level (SWL). The instantaneous free surface is located at $z' = \eta'$; and the water depth is denoted by h'. The seabed is located at $z' = (\eta' - h')$, and the local angle of the bed is given by θ'. The depth-averaged horizontal velocity is denoted by u'. The water depth below SWL at the seaward boundary is given by d_t'. The value of d_t' and the variation of θ' with respect to x' specify the slope configuration for the region $x' \geq 0$. The seabed may be assumed to be impermeable for saturated beaches. Furthermore, the vertical pressure distribution is assumed to be hydrostatic neglecting vertical fluid accelerations. This assumption may be reasonable if $(\tan\theta')^2 \ll 1$, except for the immediate vicinity of wave breaking. For the flow on the impermeable beach the governing equations for mass and x' momentum integrated from the seabed to the free surface may be expressed as

$$\frac{\partial h'}{\partial t'} + \frac{\partial}{\partial x'}(h'u') = 0 \tag{1}$$

$$\frac{\partial}{\partial t'}(h'u') + \frac{\partial}{\partial x'}(h'u'^2) = -gh'\frac{\partial \eta'}{\partial x'} - \frac{\tau_b'}{\rho} \tag{2}$$

where t' is time, g is the gravitational acceleration, τ_b' is the bottom shear stress, and ρ is the fluid density which is assumed constant. The bottom shear stress may be expressed as

$$\tau_b' = \tfrac{1}{2}\rho f'|u'|u' \tag{3}$$

where f' is the bottom friction factor which is assumed to be constant. The limited calibration made by *Kobayashi and Watson* [1987] indicated $f' = 0.05$ or less for small-scale smooth slopes without beach sediment, although the computed results were not very sensitive to the value of f'. Consequently $f' = 0.05$ is used without any further calibration for the subsequent computations.

The following dimensionless variables are introduced for the computation:

$$t = t'/T' \qquad x = x'/T'(gH')^{1/2} \qquad u = u'/(gH')^{1/2} \tag{4}$$

$$z = z'/H' \qquad h = h'/H' \qquad \eta = \eta'/H' \qquad d_t = d_t'/H' \tag{5}$$

$$\theta = (2\pi)^{1/2}\xi \qquad \xi = \sigma \tan\theta'/(2\pi)^{1/2} \tag{6}$$

$$f = \tfrac{1}{2}\sigma f' \qquad \sigma = T'(g/H')^{1/2} \tag{7}$$

where T' and H' are the characteristic wave period and height used for the normalization, respectively, θ is the normalized gradient of the slope, ξ is the local surf similarity parameter, f is the normalized friction factor, and σ is the dimensionless parameter related to wave steepness. In terms of the normalized coordinate system the seabed is located at

$$z = \int_0^x \theta\, dx - d_t \qquad x \geq 0 \tag{8}$$

which reduces to $z = (\theta x - d_t)$ for uniform slopes. For a monochromatic incident wave train, T' and H' are taken to be the period and height of the monochromatic wave. For the monochromatic wave incident on a uniform slope, ξ defined in (6) reduces to the surf similarity parameter introduced by *Battjes* [1974]. Substitution of (3), (4), (5), (6), and (7) into (1) and (2) yields

$$\frac{\partial h}{\partial t} + \frac{\partial}{\partial x}(hu) = 0 \tag{9}$$

$$\frac{\partial}{\partial t}(hu) + \frac{\partial}{\partial x}(hu^2 + \tfrac{1}{2}h^2) = -\theta h - f|u|u \tag{10}$$

which are solved numerically to obtain the variations of h and u with respect to t and x for given θ, f, initial and boundary conditions.

For the numerical computation, (9) and (10) are expressed in the conservation law form of the mass and momentum equations, except for the terms on the right-hand side of (10),

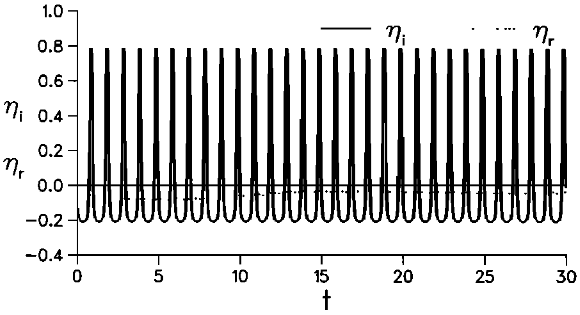

Fig. 2. Specified $\eta_i(t)$ and computed $\eta_r(t)$ at seaward boundary for test 1 of *Stive and Wind* [1982].

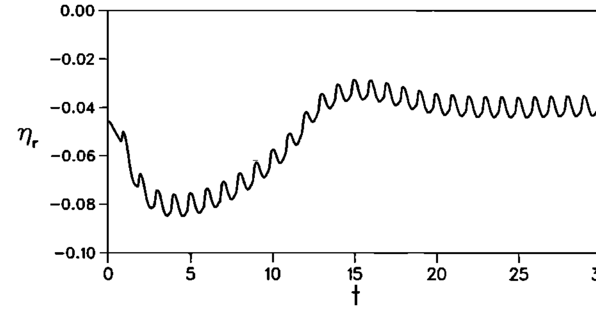

Fig. 3. Detailed variation of $\eta_r(t)$ at seaward boundary for test 1.

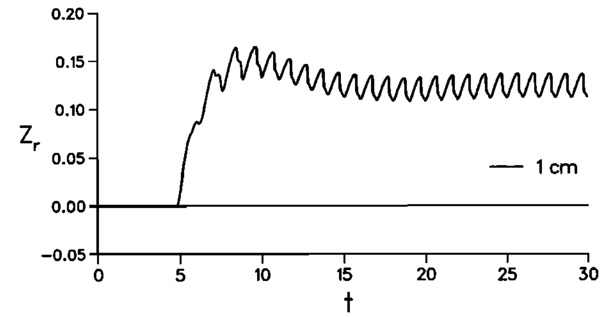

Fig. 4. Computed oscillation of 1-cm water depth on 1:40 slope for test 1.

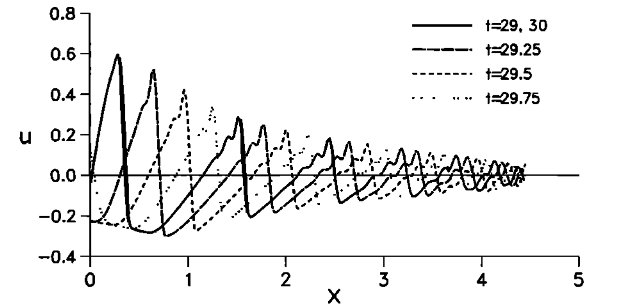

Fig. 6. Computed horizontal velocity variations during one wave period for test 1.

and solved using an explicit dissipative finite difference method of the type proposed by P. D. Lax and B. Wendroff (as cited by *Hibberd and Peregrine* [1979], *Packwood* [1980], and *Kobayashi et al.* [1987]). Use is made of a finite difference grid of constant space size Δx and constant time step Δt. Numerical methods developed for flows with shocks were recently reviewed by *Moretti* [1987]. The present numerical method is a shock-capturing method in which a wave front (shock) covers a small number of the space grid points. Inclusion of an additional dissipative term in the numerical method reduces high-frequency oscillations caused by discretization, which tend to appear at the rear of the front. The amount of this damping is controlled by the values of two damping coefficients. The values of Δt, Δx, and the damping coefficients required for the computation are specified considering the numerical stability criterion of the adopted explicit method as well as the desirable spatial and temporal accuracies [*Packwood*, 1980; *Kobayashi et al.*, 1987].

The initial time $t = 0$ for the computation marching forward in time is taken to be the time when the specified incident wave train arrives at the seaward boundary located at $x = 0$ as shown in Figure 1. The initial conditions for h and u are thus given by

$$t = 0 \qquad \eta = 0 \qquad u = 0 \qquad x \geq 0 \tag{11}$$

where the condition of $\eta = 0$ at $t = 0$ implies that the normalized depth h at $t = 0$ is equal to the normalized depth below SWL which is known for given d_t and θ and is given by $(d_t - \theta x)$ for a uniform slope.

The landward boundary on the slope is located at the moving shoreline where the water depth is zero. In reality, it is difficult to pinpoint the exact location of the moving shoreline because of the effects of surface tension and permeability neglected in this analysis. For the computation the shoreline is defined as the location where the normalized water depth h equals an infinitesimal value δ. Use is made of $\delta = 10^{-3}$, which has been used successfully for smooth slopes [*Kobayashi and Watson*, 1987]. The shoreline oscillation is computed using the predictor-corrector-smoothing procedure developed by *Hibberd and Peregrine* [1979] and *Packwood* [1980], as explained in detail by *Kobayashi et al.* [1987].

The seaward boundary is located at $x = 0$ where the normalized water depth below SWL is d_t. In order to derive an approriate seaward boundary condition, (9) and (10) are expressed in the following characteristic forms

Along $dx/dt = u + c$

$$\frac{\partial \alpha}{\partial t} + (u + c)\frac{\partial \alpha}{\partial x} = -\theta - \frac{f|u|u}{h} \tag{12}$$

Along $dx/dt = u - c$

$$\frac{\partial \beta}{\partial t} + (u - c)\frac{\partial \beta}{\partial x} = \theta + \frac{f|u|u}{h} \tag{13}$$

with

$$c = (h)^{1/2} \qquad \alpha = u + 2c \qquad \beta = -u + 2c \tag{14}$$

where α and β are the characteristic variables. It is assumed that in the vicinity of the seaward boundary $u < c$, that is, $u' < (gh')^{1/2}$ in terms of the physical variables. This assumption may be satisfied if the seaward boundary is taken to be outside the breakpoint. Then α and β represent the characteristics advancing landward and seaward, respectively, in the vicinity of the seaward boundary. Since the seaward advancing characteristics β originate from the computation domain

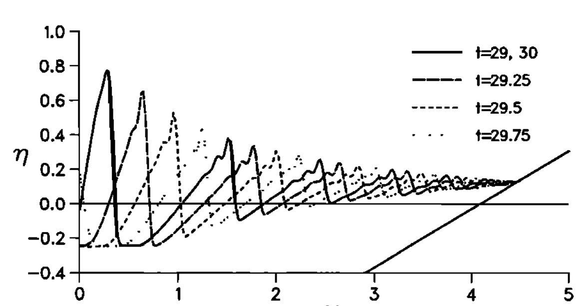

Fig. 5. Computed free surface variations during one wave period for test 1.

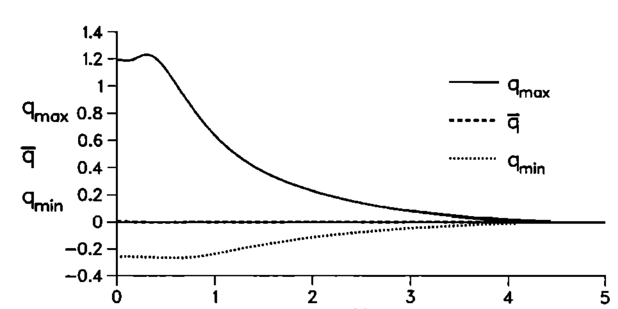

Fig. 7. Computed cross-shore variations of maximum, time-averaged, and minimum volume fluxes for test 1.

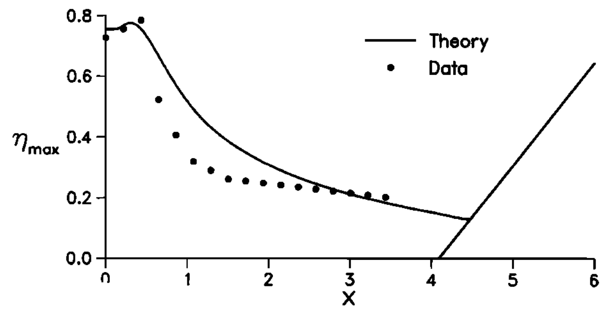

Fig. 8. Measured and computed cross-shore variations of wave crest elevation for test 1.

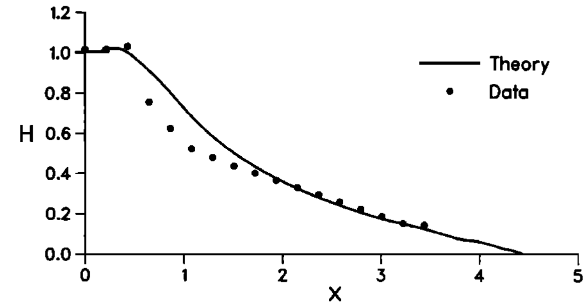

Fig. 10. Measured and computed cross-shore variations of wave height for test 1.

$x \geq 0$, (13) is discretized using a simple first-order finite difference to obtain the value of β at $x = 0$, which gives a relationship between the values of u and h at $x = 0$ [*Kobayashi et al.*, 1987]. An additional relationship is required to find u and h at $x = 0$. *Hibberd and Peregrine* [1979] prescribed the value of α associated with an incident uniform bore. This is not possible for arbitrary incident wave train since both u and h are required to specify the value of α at the seaward boundary. *Packwood* [1980] used the temporal variation of h measured inside the surf zone as input at the seaward boundary of his computation to compare the measured and computed bore transformation and shoreline oscillation on smooth gentle slopes. Packwood noticed long-period oscillations in his computed results and suggested that the seaward boundary condition based on the specification of h became partially reflecting and caused the excitation of spurious seiching motions in the computation domain.

Alternatively, the total water depth at the seaward boundary may be expressed in the form

$$h = d_t + \eta_i(t) + \eta_r(t) \qquad x = 0 \tag{15}$$

where η_i and η_r are the free surface variations at $x = 0$ normalized by the characteristic wave height H'. The incident wave train outside the breakpoint is specified by prescribing the variation of η_i with respect to $t \geq 0$. The term $\eta_r(t)$ in (15) accounts for the difference between the actual value $\eta = (\eta_i + \eta_r)$ at $x = 0$ and the prescribed value η_i. For reflective slopes, $\eta_r(t)$ may be regarded as the normalized free surface variation associated with the reflected wave train, neglecting the nonlinear interaction of the incident and reflected waves at the seaward boundary. For dissipative slopes, wave reflection may be negligible, but $\eta_r(t)$ accounts for the difference between the actual and prescribed free surface variations which may arise from the transient long-period waves generated in this time domain computation starting from the initial conditions given by (11) as well as the other secondary effects excluded from the prescribed variation of $\eta_i(t)$. Considering all the possibilities for arbitrary slope geometry, it is difficult to specify the unknown temporal variation of $\eta_r(t)$ in a rigorous manner.

It may be reasonable to express $\eta_r(t)$ at $x = 0$ in terms of the value of the seaward advancing characteristics, β, at $x = 0$, computed using (13). Using (14) and (15) with the assumption that d_t is sufficiently large relative to the value of $(\eta_i + \eta_r)$, the value of β at $x = 0$ may be approximated by

$$\beta \simeq -u + 2(d_t)^{1/2} + \frac{\eta_i + \eta_r}{(d_t)^{1/2}} \qquad x = 0 \tag{16}$$

Using the approximations based on linear long-wave theory, u in (16) may be expressed as

$$u \simeq \frac{\eta_i - \eta_r}{(d_t)^{1/2}} + \bar{u}_t \qquad x = 0 \tag{17}$$

where $\bar{u}_t$ is the time-averaged horizontal velocity at $x = 0$ and may be regarded as a nonlinear correction term in (17). Substitution of (17) into (16) yields the following approximate expression of η_r in terms of the value of β at $x = 0$:

$$\eta_r(t) \simeq \tfrac{1}{2}(d_t)^{1/2}\beta(t) - d_t - C_t \qquad x = 0 \tag{18}$$

$$C_t = -\tfrac{1}{2}(d_t)^{1/2}\bar{u}_t \tag{19}$$

where the nonlinear correction term C_t in (18) was not included in the numerical model of *Kobayashi et al.* [1987]. Substitution of (18) into (15) yields the value of h at $x = 0$ for given $\eta_i(t)$, and the value of u at $x = 0$ is obtained from $u = (2h^{1/2} - \beta)$ at $x = 0$. It should be noted that the approximate equations (16) and (17) are used only for deriving (18). Appropriateness of (18) used for the computation may be evaluated by comparing the computed and measured temporal variations of

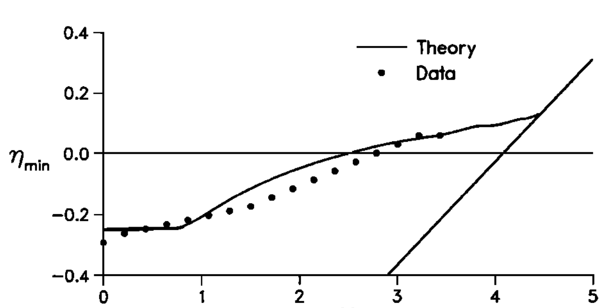

Fig. 9. Measured and computed cross-shore variations of wave trough elevation for test 1.

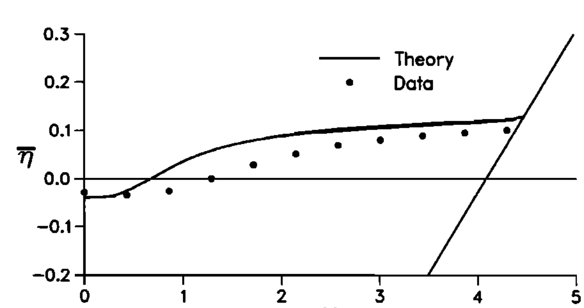

Fig. 11. Measured and computed cross-shore variations of mean water level for test 1.

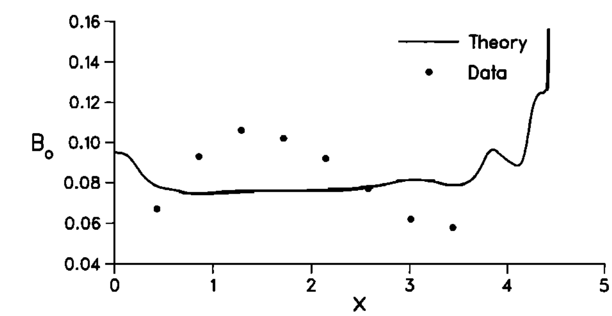

Fig. 12. Measured and computed cross-shore variations of parameter B_0 for test 1.

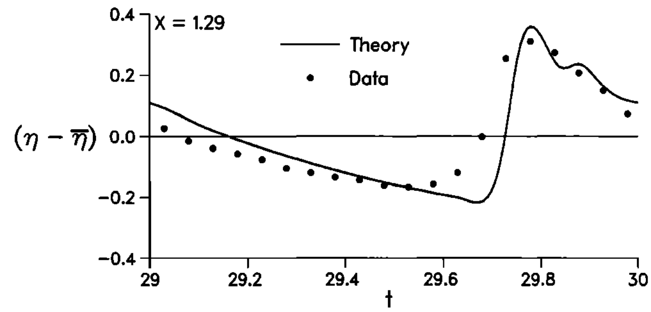

Fig. 14. Measured and computed wave profiles at $x = 1.29$ for test 1.

$\eta_r(t)$ as well as by comparing the computed reflection coefficients with empirical formulas such as those proposed by *Battjes* [1974] and *Seelig* [1983]. Use of (18) with $C_t = 0$ was shown to yield satisfactory agreement for the comparisons made for steep slopes in the range of $\xi \gtrsim 1$ and $d_t \gtrsim 3$ by *Kobayashi et al.* [1987], *Kobayashi and Greenwald* [1986, 1988], and *Kobayashi and Watson* [1987]. Furthermore, the temporal variations of h and u on steep slopes computed for the periodic variations of $\eta_i(t)$ specified by cnoidal or Stokes second-order wave theory [e.g., *Svendsen and Brink-Kjaer*, 1972; *Dean and Dalrymple*, 1984] became periodic after several wave periods without the spurious long-period oscillations noticed by *Packwood* [1980]. The use of cnoidal or Stokes wave theory for specifying $\eta_i(t)$ at the toe of a steep slope was theoretically inconsistent but necessary since the finite amplitude, shallow water equations used in the computation domain do not have a periodic solution for the wave of constant form [e.g., *Peregrine*, 1967].

In the following the nonlinear correction term C_t included in (18) is shown to improve the prediction of wave setup on a gentle slope. This term is also shown to be negligible for the previous comparisons made for steep slopes. The time-averaged mass and momentum equations corresponding to (9) and (10) may be expressed as

$$\overline{hu} = 0 \tag{20}$$

$$\frac{d}{dx}\left[\overline{hu^2} + \tfrac{1}{2}\overline{(\eta - \bar{\eta})^2}\right] = -\bar{h}\frac{d\bar{\eta}}{dx} - f\overline{|u|u} \tag{21}$$

where the overbar denotes time averaging and $\bar{\eta}$ is the vertical difference between the mean and still water levels with η and h being defined in Figure 1. Use is made of the condition of no flux into the impermeable slope to derive (20). The left-hand side of (21) is the normalized gradient of the cross-shore radiation stress [e.g., *Svendsen et al.*, 1987] under the assumption of vertical uniformity and hydrostatic pressure. In this paper the computed temporal variations of h and u at given location are used to calculate the cross-shore variations of the time-averaged quantities such as $\bar{\eta}$ and $\bar{u}$ without using (20) and (21). The no flux condition given by (20) is used to check the accuracy of the computation.

Rearranging (20), the time-averaged horizontal velocity $\bar{u}$ can be expressed as

$$\bar{u} = -\overline{(\eta - \bar{\eta})(u - \bar{u})}(\bar{h})^{-1} \tag{22}$$

For gentle slopes with little wave reflection, $(\eta - \bar{\eta})$ and $(u - \bar{u})$ are expected to be in phase, resulting in $\bar{u} < 0$ from (22). The computed seaward velocity $\bar{u}$ is expected to be smaller than the undertow flowing seaward below the wave trough since the present model does not account for the vertical variation of the time-averaged horizontal velocity. The value of $\bar{u}$ at $x = 0$ (i.e., $\bar{u}_t$) is required to find C_t using (19). This will require an iteration since $\bar{u}_t$ is unknown. An approximate value of $\bar{u}_t$ may be found using (22) with the assumption of incident monochromatic linear long wave at the seaward boundary whose height and period are taken to be H' and T' used in (4), (5), and (7). Under this assumption, $(\eta - \bar{\eta}) \simeq \cos(2\pi t)/2$, $(u - \bar{u}) \simeq (\eta - \bar{\eta})/(d_t)^{1/2}$ and $\bar{h} \simeq d_t$ at $x = 0$. For gentle slopes with little wave reflection the approximate values of $\bar{u}_t$ and C_t may hence be estimated as

$$\bar{u}_t \simeq -(8d_t^{3/2})^{-1} \qquad C_t \simeq (16d_t)^{-1} \tag{23}$$

Since (23) yields $C_t > 0$, the value of $\eta_r(t)$ computed using (18) will be reduced. For steep slopes with significant wave reflection for which η_r is on the order of unity, it might be more reasonable to assume that $\bar{u}_t \simeq 0$ and $C_t \simeq 0$, but the effect of C_t on η_r in (18) is very small. For the previous comparisons made for steep slopes, $d_t \gtrsim 3$ and hence $C_t \lesssim 0.02$. If the value of d_t is reduced from three, the value of C_t will affect the wave setup $\bar{\eta}$, which is an important consideration for gentle slopes. The wave setup or setdown at $x = 0$ is given by $\bar{\eta} = (\bar{\eta}_i + \bar{\eta}_r)$

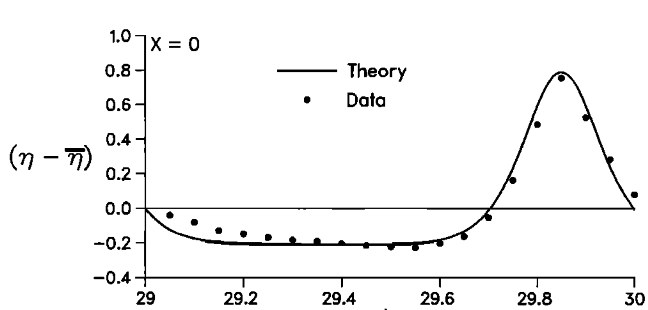

Fig. 13. Measured and computed wave profiles at $x = 0$ for test 1.

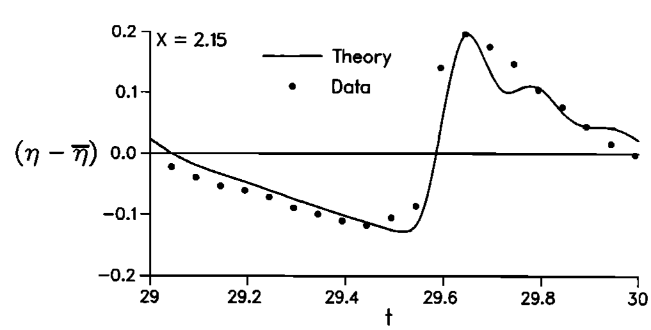

Fig. 15. Measured and computed wave profiles at $x = 2.15$ for test 1.

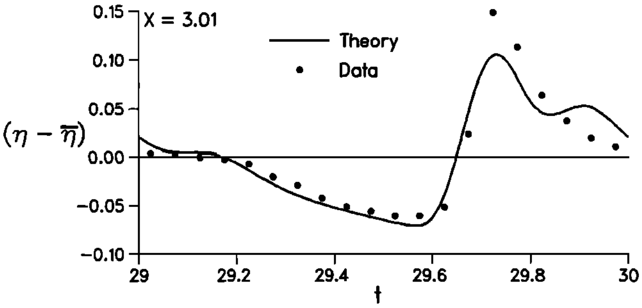

Fig. 16. Measured and computed wave profiles at $x = 3.01$ for test 1.

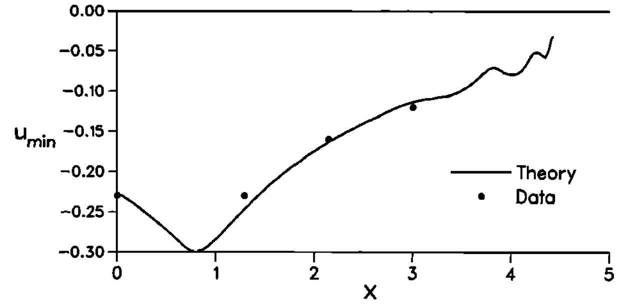

Fig. 18. Measured and computed cross-shore variations of minimum horizontal velocity for test 1.

at $x = 0$. Substituting (16) into (18), the following time-averaged equation is obtained:

$$\bar{\eta}_r \simeq \bar{\eta}_i - (d_t)^{1/2}\bar{u}_t - 2C_t \tag{24}$$

The incident monochromatic wave train at the seaward boundary may be specified to satisfy the condition $\bar{\eta}_i = 0$ so as to limit the computation to the region $x \geq 0$. For $\bar{\eta}_i = 0$, $\bar{\eta}_r \simeq (8d_t)^{-1}$ if $C_t = 0$ and $\bar{\eta}_r \simeq 0$ if C_t is given by (19). The wave setup data of *Stive and Wind* [1982] indicated small wave setdown outside the breakpoint on a gentle slope. Without the term C_t in (18) the model would predict too large a setup, $(\bar{\eta}_i + \bar{\eta}_r) \simeq (8\ d_t)^{-1}$, at the seaward boundary where $d_t = 1.38$ is used, as will be explained in the subsequent comparison. In other words, C_t is related to the boundary condition required for solving (21) to obtain the cross-shore variation of $\bar{\eta}$. For simplicity, use is made of $C_t = (16d_t)^{-1}$ in (18) for all the computed results presented in this paper. To eliminate the uncertainties associated with the approximate equation (18), it may be required to match the solution on the basis of the finite amplitude, shallow water equations with that based on the Boussinesq equations outside the breakpoint. This is beyond the scope of this paper.

WAVE TRANSFORMATION ON GENTLE SLOPES

Comparison is made with the comprehensive measurements of test 1 presented by *Stive* [1980] and *Stive and Wind* [1982]. Some of these measurements were also reanalyzed and used in the paper of *Svendsen* [1984*b*]. In this test the incident monochromatic wave with the period $T' = 1.79$ s broke as spilling breakers on the plane concrete beach of the slope cot $\theta' = 40$. The seaward boundary for the computation is taken to be at the still water depth $d_t' = 0.2375$ m, where the near-breaking wave profile was shown to be similar to the cnoidal wave profile. The measured wave height at the seaward boundary was given by $H' = 0.172$ m. The dimensionless parameters defined in (5), (6), and (7) are given by $d_t = 1.38$, $\theta = 0.338$, $\xi = 0.135$, $f = 0.338$, and $\sigma = 13.5$ for the test. The temporal variation of the incident wave profile $\eta_i(t)$ at $x = 0$ whose height and period are unity is specified using cnoidal wave theory as explained by *Kobayashi and DeSilva* [1987] except that the dispersion relationship used in their paper is modified slightly to make it identical to that given by *Svendsen and Brink-Kjaer* [1972]. For the incident cnoidal wave at $x = 0$, $L = 13.1$ and $U_r = 124$ where L is the normalized wavelength defined as $L = (L'/d_t')$ with L' being the wavelength, and U_r is the Ursell number given by $U_r = (L^2/d_t)$. Use of the finite amplitude, shallow water equations may be appropriate in the region $x \geq 0$. The computation for this test is performed successfully using $\Delta x = 2.04 \times 10^{-2}$, $\Delta t = 3.33 \times 10^{-3}$, and the damping coefficients of two. These values are typical for the computed results presented herein, except that for steep slopes smaller values of Δt are found to be required for the numerical statility. The computed results for test 1 are shown in Figures 2–19 and explained in the following discussion.

Figure 2 shows the periodic cnoidal wave profile $\eta_i(t)$ with $\bar{\eta}_i = 0$ specified at $x = 0$ and the temporal variation of $\eta_r(t)$ computed using (18) with $C_t = (16d_t)^{-1}$, where the normalized wave period is unity. The normalized free surface variation relative to SWL is given by $\eta = (\eta_i + \eta_r)$ at $x = 0$. The detailed variation of $\eta_r(t)$ is shown in Figure 3. The depression of η_r during the transient period $0 \leq t \lesssim 15$ appears to be related to the depression of the mean water level under large waves [*Longuet-Higgins and Stewart*, 1962], since the incident wave train initially propagates into the region of no wave action. The temporal variation of $\eta_r(t)$ for $t \gtrsim 20$ consists of steady and oscillatory components. The steady component is the wave setdown $\bar{\eta}$ at $x = 0$, while the oscillatory component is associated with the reflected wave. Since the normalized incident wave height is unity, the height of this oscillatory compo-

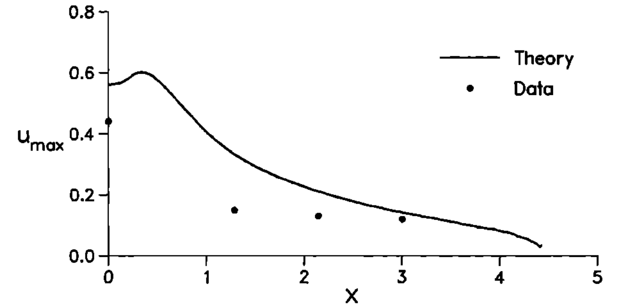

Fig. 17. Measured and computed cross-shore variations of maximum horizontal velocity for test 1.

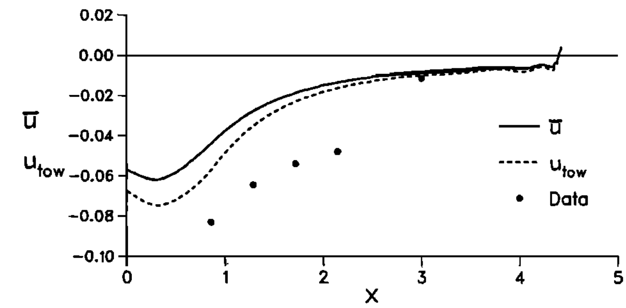

Fig. 19. Cross-shore variations of computed time-averaged horizontal velocity and measured undertow for test 1.

TABLE 1. Summary of Seven Cases Compared With Empirical Formulas of *Guza and Bowen* [1976] and *Guza et al.* [1984]

Case	H', cm	ξ	d_t	σ	L	U_r	r
1	1.0	4.24	38	86	14	4.8	0.57
2	1.3	3.72	29	76	14	6.3	0.50
3	2.0	3.00	19	61	14	9.7	0.36
4	2.6	2.63	15	54	14	13	0.28
5	5.5	1.81	6.9	37	14	27	0.08
6	8.0	1.50	4.8	31	14	41	0.08
7	10.0	1.34	3.8	27	14	52	0.09

nent may be taken to be the wave reflection coefficient, which is approximately 0.01.

On the other hand, the computational shoreline is defined by $h = \delta$ with $\delta = 10^{-3}$ in this paper. The oscillation of the specified dimensional water depth on the slope denoted by δ_r' can be computed using the computed variation of h with respect to x and t as long as $\delta_r \geq \delta$, where $\delta_r = \delta_r'/H'$. The present numerical model was shown to yield satisfactory agreement with the empirical formula of *Ahrens and Martin* [1985] for the maximum runup of monochromatic waves observed visually on smooth steep slopes in small-scale tests if δ_r' is taken to be of the order of 0.1 cm or greater [*Kobayashi and Watson*, 1987]. Consequently, computation is made of the shoreline oscillations on the slope for $\delta_r' = 0.1$, 0.5, and 1 cm, that is, $\delta_r = 0.0058$, 0.029, and 0.058, respectively. The computed oscillation for given δ_r' is plotted in the form of Z_r as a function of t where Z_r is the elevation above SWL normalized by the incident wave height H'. Figure 4 shows the computed variation of Z_r for $\delta_r' = 1$ cm with respect to the normalized time t. The specified incident wave train arrives at the still water level shoreline at $t \simeq 5$. After the initial transient oscillation the temporal variation of Z_r for $t \gtrsim 25$ is composed of steady and oscillatory components. The steady component is the normalized setup on the slope denoted by $\bar{Z}_r$, while the oscillatory component is the normalized swash about the setup level. The variation of Z_r for $\delta_r' = 0.1$ and 0.5 cm, which are not plotted in Figure 4 for simplicity, essentially follow that for $\delta_r' = 1$ cm, except that the swash decreases as the value of δ_r' is reduced. The computed swash for $\delta_r' = 0.1$ cm is almost indistinguishable. The setup $\bar{Z}_r$ is essentially the same in the range of $\delta_r' = 0.1$–1.0 cm. The normalized swash height, which is 0.02 even for $\delta_r' = 1$ cm, is small relative to the normalized setup $\bar{Z}_r = 0.13$ for this test with $\xi = 0.135$. The computed results are hence consistent with the empirical results discussed by *Battjes* [1974] and the hypothesis of saturation proposed by *Huntley et al.* [1977].

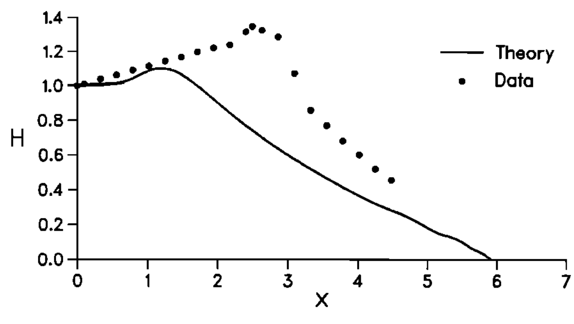

Fig. 20. Measured and computed cross-shore variations of wave height for the test of *Hansen and Svendsen* [1984].

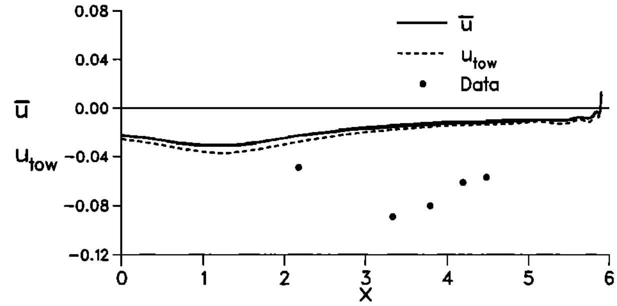

Fig. 21. Cross-shore variations of computed time-averaged horizontal velocity and measured undertow by *Hansen and Svendsen* [1984].

Figure 3 and 4 suggest that the response time for the gentle slope is much greater than the incident wave period and appears to be of the order of the time scale of the surf beat motion on a gentle slope. *Stive and Wind* [1982] stated that their measurements were made after at least 10 min of wave generation to allow for the decay of initial low-frequency effects. Figures 3 and 4 indicate that the computed results during one wave period $29 \leq t \leq 30$ should be periodic without initial low-frequency effects. Figures 5 and 6 show the computed cross-shore variations of the normalized free surface elevation η above SWL and the normalized horizontal velocity u at $t = 29$, 29.25, 29.5, 29.75, and 30, respectively. The slope shown in Figure 5 is located at $z = (\theta x - d_t)$ in terms of the normalized coordinate system. In Figures 5 and 6 the computed cross-shore variations of η and u at $t = 29$ and 30 are identical, indicating the establishment of the periodicity before $t = 29$. Moreover, the transformation from the near-breaking wave specified at $x = 0$ to the sawtooth-shaped bore in the inner surf zone in Figure 5 appears to be realistic except for the details of wave breaking as compared with the typical wave shapes depicted by *Svendsen et al.* [1978] and *Flick et al.* [1981].

In the following the computed variations of h and u during one wave period $29 \leq t \leq 30$ are used to make comparisons with the measurements of test 1. Expressing the volume flux as $q = hu$, the maximum, time-averaged and minimum values of q at given x during $29 \leq t \leq 30$ are denoted by q_{max}, $\bar{q}$, and q_{min}, respectively. The computed cross-shore variations of q_{max}, $\bar{q}$, and q_{min} are plotted in Figure 7 to show that the computed results satisfy the condition of $\bar{q} = 0$ given in (20) almost exactly. In Figure 7 the variation of $\bar{q}$ starts from 5×10^{-4} at $x = 0$, decreases to -3×10^{-3} at $x = 0.5$, and approaches zero rapidly with the increase of x from 0.5. This indicates the degree of the computational accuracy expected for the com-

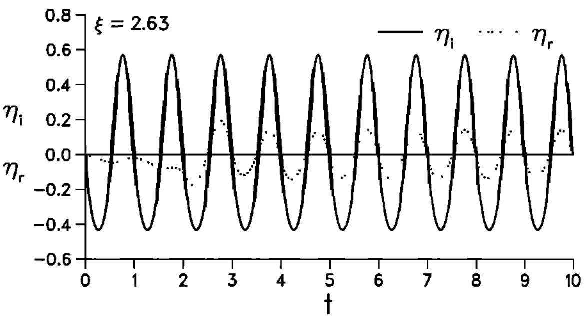

Fig. 22. Specified $\eta_i(t)$ and computed $\eta_r(t)$ for case 4 compared with empirical formulas of *Guza and Bowen* [1976] and *Guza et al.* [1984].

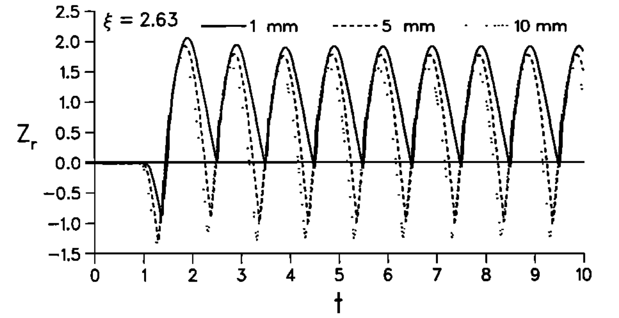

Fig. 23. Computed oscillations of 1, 5, and 10 mm water depth on 1:8.14 slope for case 4.

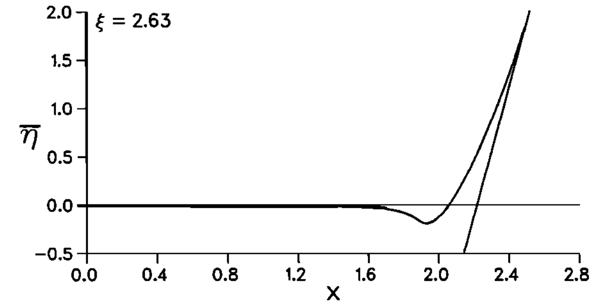

Fig. 25. Computed cross-shore variation of mean water level for case 4.

puted time-averaged quantities presented in this paper. The time-averaged values are found to require better computational accuracy than the maximum and minimum values. Denoting the maximum and minimum values of η at given x during $29 \leq t \leq 30$ by η_{max} and η_{min}, respectively, the computed cross-shore variations of η_{max} and η_{min} are compared with the measured crest and trough envelopes as shown in Figures 8 and 9, respectively. Figure 10 shows the comparison for the normalized local wave height H, defined as $H = (\eta_{max} - \eta_{min})$. The data points shown in Figures 8, 9, and 10 are the values read from the wave envelope drawn in Figure 4 of *Stive and Wind* [1982]. The breakpoint in these figures is located at $x \simeq 0.4$. The effects of wave shoaling and breaking on the wave envelope are well predicted for this test. The apparent coincidence of the computed and measured breakpoint locations may be related to the location of the seaward boundary chosen for the computation, as will be discussed in connection with the computed results for the test of *Hansen and Svendsen* [1984].

Figure 11 shows the measured and computed cross-shore variations of the time-averaged free surface elevation $\bar{\eta}$ above SWL. It should be noted that the computed mean water level shown in Figure 11 would move vertically upward with little change of its shape by the amount of approximately $(8d_t)^{-1} = 0.09$ if $C_t = 0$ were assumed in (18) instead of $C_t = (16d_t)^{-1}$ used for the present computation. The nonlinear correction term C_t introduced in (18) definitely improves the agreement for the mean water level, although the other computed quantities are found to be affected little by this term. The computed mean water level shown in Figure 11 rises too rapidly landward of the breakpoint, as was the case with the previous comparisons made by *Stive and Wind* [1982] and *Svendsen* [1984*a*]. Figure 12 shows the measured and computed cross-shore variations of the parameter B_0 introduced by *Svendsen* [1984*a*, 1984*b*], which can be expressed as $B_0 = [\overline{\eta^2} - (\bar{\eta})^2]/H^2$ in the present notation. The agreement shown in Figure 12 may not be good, but the measured values of B_0 presented by *Svendsen* [1984*a*] were scattered around 0.07–0.08 in the inner surf zone.

On the other hand, Figures 13, 14, 15, and 16 show the comparison between the measured wave profile and the computed temporal variation of $(\eta - \bar{\eta})$ during $29 \leq t \leq 30$ at $x = 0$, 1.29, 2.15, and 3.01, respectively. The data points shown in these figures are read from the wave profiles shown in Figure 6 of *Stive* [1980]. Each of the measured profiles was plotted about its crest, which was taken to be at $t = 0$. Consequently, the measured profiles shown in Figures 13, 14, 15, and 16 are plotted such that the computed and measured wave crests occur at the same time. This assumes that the numerical model can predict the velocity of wave crest propagation from $x = 0$ to the specified location exactly. Figure 13 indicates that the measured wave profile at $x = 0$ is well approximated by the cnoidal wave profile η_i specified at $x = 0$, where $(\eta - \bar{\eta}) \simeq \eta_i$ at $x = 0$, since $\bar{\eta}_i = 0$ and $\eta_r \simeq \bar{\eta}_r$ during $29 \leq t \leq 30$, as shown in Figure 3. Figures 14, 15, and 16 show that the numerical model can predict the measured transformation from the symmetric profile at $x = 0$ outside the breakpoint to the sawtooth profiles in the inner surf zone, although some numerical oscillations are present at the rear of the wave front.

As for the prediction of the velocity field, the numerical model is less satisfactory since it predicts only the depth-averaged horizontal velocity u. The maximum, time-averaged, and minimum values of the computed temporal variation of u at given x during $29 \leq t \leq 30$ are denoted by u_{max}, $\bar{u}$, and u_{min}, respectively. Figure 7 of *Stive* [1980] showed that the maximum and minimum horizontal velocities measured at several elevations did not change much vertically. The average of the measured velocities may hence be regarded as the depth-averaged velocity. Figures 17 and 18 show the computed

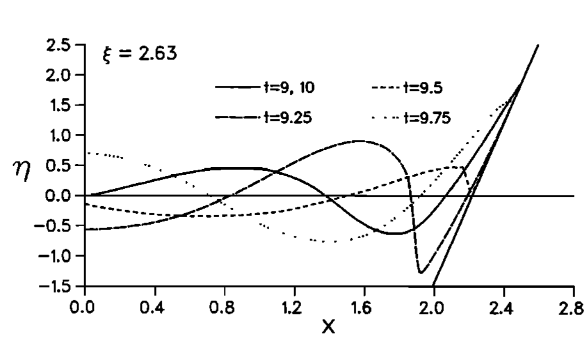

Fig. 24. Computed free surface variations for case 4.

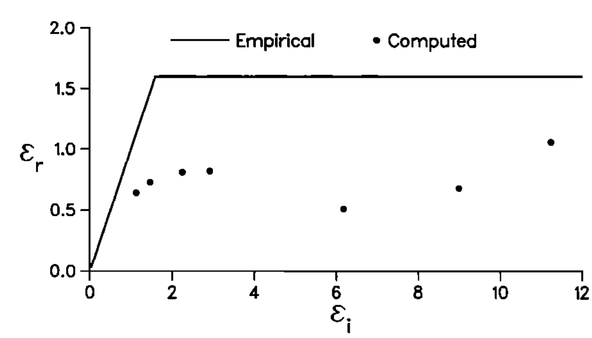

Fig. 26. Comparison of computed reflection coefficients with empirical formula.

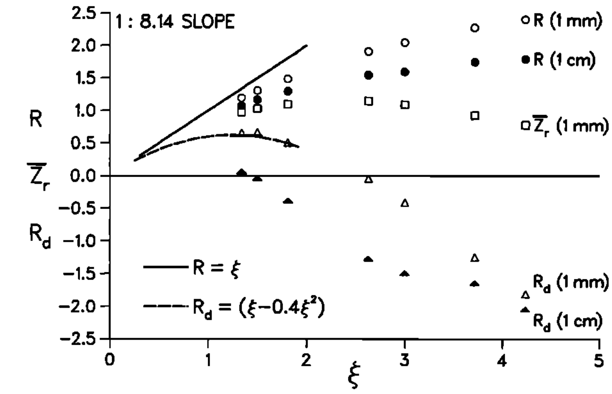

Fig. 27. Computed maximum runup R, setup $\bar{Z}_r$, and rundown R_d for seven cases.

TABLE 2. Summary of Nine Runs for 1:8 Smooth Slope Tests

Run	T', s	H', cm	ξ	d_t	σ	L	U_r
S1	1.2	8.80	0.63	4.5	13	4.8	5.1
S2	2.0	6.60	1.2	6.1	24	9.2	14
S3	3.2	5.43	2.1	7.4	43	15	32
G1	2.15	14.50	0.88	2.8	18	11	40
G2	3.0	9.91	1.5	4.0	30	14	51
G3	3.2	8.38	1.7	4.8	35	15	50
B1	1.2	9.48	0.61	4.2	12	4.8	5.6
B2	2.0	7.55	1.1	5.3	23	9.2	16
B3	3.2	5.45	2.1	7.3	43	15	32

cross-shore variations of u_{max} and u_{min}, respectively, together with the data points corresponding to the average of the measured velocities at given x. The numerical model appears to overpredict the maximum horizontal velocity even at $x = 0$ and predict the minimum horizontal velocity well. *Flick et al.* [1981] suggested, on the basis of previous studies, that most wave theories would considerably overestimate the horizontal velocity under the crest of near-breaking waves generated in laboratories which were likely to be contaminated with free second-harmonic waves [*Madsen*, 1971]. *Stive* [1980] and *Stive and Wind* [1982] stated that monochromatic waves with minimal free second-harmonic waves were generated for the test under consideration. Comparison of the velocity data with cnoidal and linear wave theories was made by *Stive* [1980]. For the near-breaking wave at $x = 0$, cnoidal wave theory overestimated u_{max} and estimated u_{min} well, whereas linear wave theory estimated u_{max} well and overestimated u_{min}. For the breaking waves in the inner surf zone, linear wave theory estimated u_{max} and u_{min} reasonably well using the measured local wave height. However, existing wave theories cannot predict the asymmetry about the crest associated with the sawtooth profile in the inner surf zone [*Flick et al.*, 1981].

Figure 19 shows the computed cross-shore variation of the time-averaged horizontal velocity $\bar{u}$ together with the data points for test 1 corresponding to the average of the measured undertow velocities below the wave trough at given x. The data points in Figure 19 are read from Figure 8 of *Svendsen* [1984*b*], which showed the vertical variation and scatter of the undertow velocities measured at different elevations. The more recent data of *Hansen and Svendsen* [1984] as well as the undertow analysis including the effect of the bottom boundary layer by *Svendsen et al.* [1987] indicated that the undertow velocity below the wave trough should vary less vertically. Considering the limitation of the numerical model based on the assumption of vertical uniformity, Figure 19 should be interpreted to show that the numerical model predicts the order-of-the-magnitude of the undertow and the landward decrease of the undertow inside the breakpoint at $x \simeq 0.4$. The dotted line denoted by u_{tow} in Figure 19 corresponds to the value of $\bar{u}$ multiplied by the ratio between the depth below the computed mean water level and the depth below the computed wave trough level. The difference between these two depths is not sufficient to explain the underprediction of the undertow as shown in Figure 19.

Comparison is also made with the undertow measurements conducted by *Hansen and Svendsen* [1984], who stated that the wave period $T' = 2$ s, the wave height $H' = 0.12$ m, and the water depth $d_t' = 0.36$ m in front of the sloping beach with cot $\theta' = 34.25$. The seaward boundary for the computation is taken at the toe of this slope, since no information was given of the measured wave profiles immediately seaward of the breakpoint. The dimensionless parameters defined in (5), (6), and (7) are given by $d_t = 3.00$, $\theta = 0.528$, $\xi = 0.211$, $f = 0.452$, and $\sigma = 18.1$ for this test. The temporal variation of $\eta_i(t)$ at the seaward boundary located at $x = 0$ is specified using cnoidal wave theory. The wavelength normalized by d_t' and the Ursell number are given by $L = 10.2$ and $U_r = 34.4$, respectively. The computed results are plotted in the same manner as those shown above, although comparisons with the data for this test are limited to η_{max}, η_{min}, H, and $\bar{u}$ [*DeSilva*, 1988]. Figure 20 shows the measured and computed cross-shore variations of the normalized local wave height, $H = (\eta_{max} - \eta_{min})$, for this test. The data points in Figure 20 are read from the curve drawn in Figure 8 of *Hansen and Svendsen* [1984]. The numerical model predicts the increase of H due to wave shoaling well, but the predicted location of the breakpoint is too far seaward. The selected location of the seaward boundary may be too far seaward for the finite amplitude, shallow water

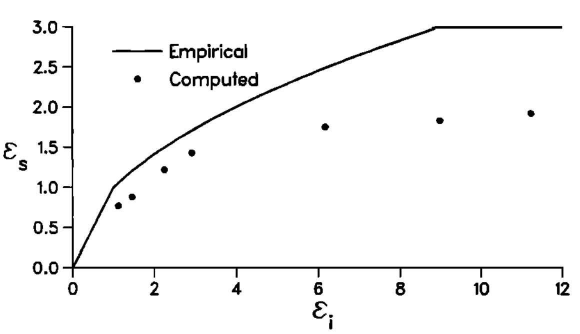

Fig. 28. Comparison of computed swash heights with empirical formula.

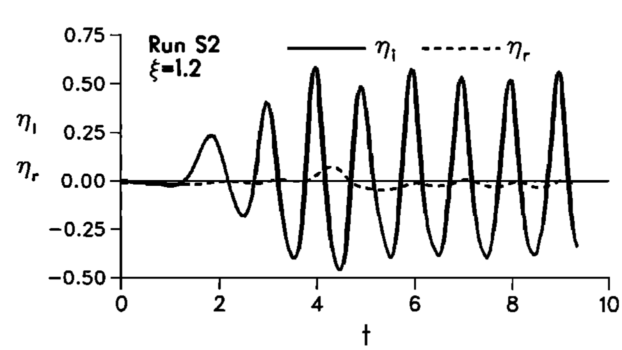

Fig. 29. Measured $\eta_i(t)$ and computed $\eta_r(t)$ for run S2.

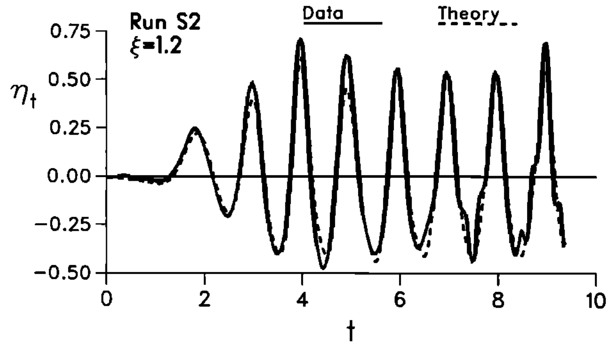

Fig. 30. Measured and computed free surface oscillation for run S2.

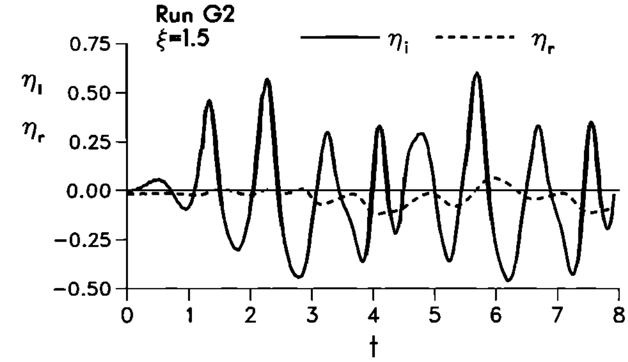

Fig. 32. Measured $\eta_i(t)$ and computed $\eta_r(t)$ for run G2.

equations used for the model, which do not include the effect of the vertical fluid acceleration on the pressure, unlike the Boussinesq equations [*Peregrine*, 1967], and appear to be incapable of predicting the wave shoaling without wave breaking over a long distance on the gentle slope. It should be noted that the previous comparisons made for steep slopes with $d_t \gtrsim 3$ [e.g., *Kobayashi et al.*, 1987] did not reveal this problem, since the distance between the toe of a steep slope and the breakpoint is relatively short. As a result, the agreements for η_{max} and η_{min} for this test are not as good as those shown in Figures 8 and 9. Figure 21 shows the computed cross-shore variation of the time-averaged horizontal velocity $\bar{u}$ together with the undertow data for this test in the same manner as Figure 19. The agreement in Figure 21 is similar to that in Figure 19, although the vertical variation of the measured undertow velocities for this test is less than that for test 1 of *Stive and Wind* [1982].

WAVE REFLECTION AND SWASH OSCILLATION ON STEEP SLOPES

First, comparison is made with the semiempirical formulas for wave reflection and swash heights proposed by *Guza et al.* [1976, 1984], who performed a laboratory and theoretical study of the transition from strongly reflected surging to dissipative plunging breakers on a relatively steep plane beach with $\theta' = 7°$, i.e., cot $\theta' = 8.14$. Incident wave periods of 2.39, 2.76, and 3.39 s were studied in detail. For simplicity the period $T' = 2.76$ s is assumed in the following comparison. Measurements of free surface oscillations were made along the section of the beach where the water depth ranged from 65 cm to approximately 10 cm. Higher harmonics were removed from the measurements to compare the free surface displacements at the primary frequency with linear solutions for fully and partly reflected waves. The wave runup and rundown measurements were done with a meter stick. A direct comparison of the present numerical model with these measurements is not possible since the model is based on the finite amplitude, shallow water equations, including the effect of bottom friction, that are solved numerically in the time domain. In order to make an approximate comparison the water depth at the seaward boundary of the numerical model may be taken as $d_t' = 38$ cm, which is the average depth between 65 cm and 10 cm. Varying the incident wave height H' in the range 1–10 cm, seven cases are selected for the subsequent computation and comparison, as summarized in Table 1. The surf similarity parameter ξ is reduced from $\xi = 4.24$ for case 1 to $\xi = 1.34$ for case 7, corresponding to the transition from surging waves to plunging breakers [*Battjes*, 1974]. The parameters d_t and σ whose values are listed in Table 1 determine the values of the normalized wavelength L and the Ursell number U_r as well as the normalized incident wave profile $\eta_i(t)$ at the seaward boundary, estimated using cnoidal wave theory for $U_r \geq 26$ and Stokes second-order wave theory for $U_r < 26$ [*Kobayashi et al.*, 1987]. The parameters θ and f whose values are not listed in Table 1 can be calculated from $\theta = (2\pi)^{1/2}\xi$ and $f = (\sigma f'/2)$, where use is made of $f' = 0.05$. The computed reflection coefficient r given in Table 1 depends on ξ, d_t, σ, and f', although the surf similarity parameter ξ is normally assumed to be the most important [e.g., *Battjes*, 1974; *Seelig*, 1983]. It should be mentioned that the numerical model may be applied to these cases with $L = 14$, although the values of d_t are relatively large.

Figures 22–25 show the computed results for case 4. These figures and similar figures plotted for each of the other cases indicate that the periodicity of the wave field is established well before $t = 9$ for all the seven cases selected for the 1:8.14 slope. Figure 22 shows the specified incident wave profile $\eta_i(t)$ and the computed reflected wave profile $\eta_r(t)$ at the seaward

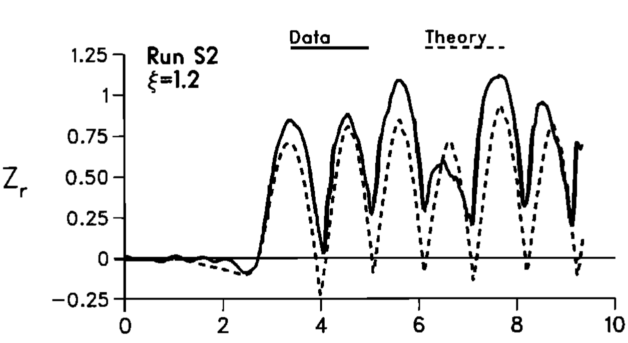

Fig. 31. Measured and computed shoreline oscillation for run S2.

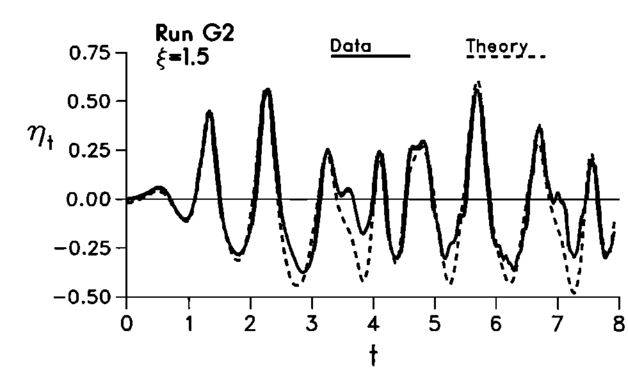

Fig. 33. Measured and computed free surface oscillation for run G2

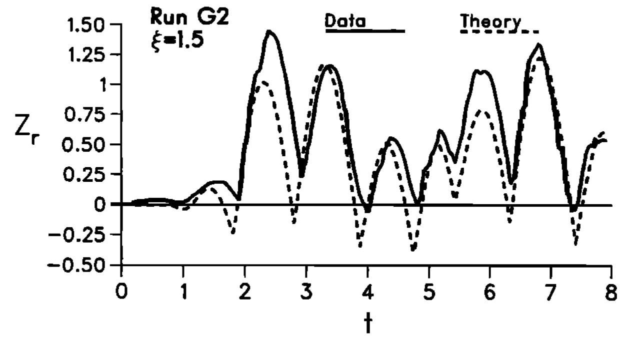

Fig. 34. Measured and computed shoreline oscillation for run G2.

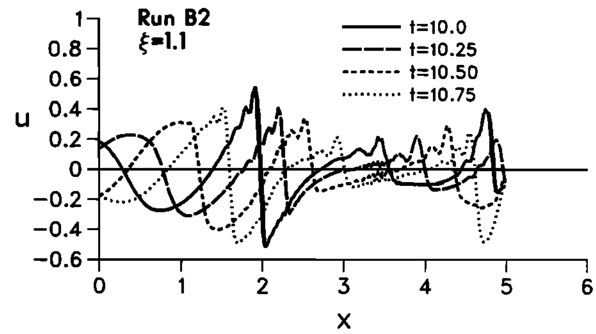

Fig. 36. Computed horizontal velocity variations over an idealized bar for run B2.

boundary for case 4. For these cases the oscillatory component of $\eta_r(t)$ after the establishment of periodicity is dominant, unlike the computed variation of $\eta_r(t)$ shown in Figures 2 and 3 for the 1:40 slope. The reflection coefficient r listed in Table 1 is taken as the height of the oscillatory component of $\eta_r(t)$ for each case, where the normalized height of $\eta_i(t)$ is unity. Figure 23 shows the computed shoreline oscillations expressed in terms of the normalized elevation Z_r above SWL corresponding to the water depth $\delta_r' = 1$, 5, and 10 mm. In comparison to the computed shoreline oscillation on the 1:40 slope shown in Figure 4 the swash component after the establishment of periodicity is much larger for the 1:8.14 slope. Moreover, the swash on the relatively steep slope is sensitive to the value of δ_r' especially during wave downrush. This is because a thin layer of water remains on the relatively steep slope during wave downrush as shown in Figure 24, which depicts the computed cross-shore variations of the normalized free surface variation η above SWL at $t = 9$, 9.25, 9.5, 9.75, and 10. The straight solid line in Figure 24 is the 1:8.14 slope located at $z = (\theta x - d_t)$, where $\theta = 6.6$ and $d_t = 14.6$ for case 4. The computed variations of η for the other cases are similar to those shown in Figure 24 except that the wave front landward of the wave crest becomes steeper as the value of ξ is reduced. It should be mentioned that the present numerical model is not capable of describing detailed behavior of plunging breakers. Comparison between Figures 5 and 24 indicates that the number of waves in the surf zone decreases as the surf similarity parameter ξ is increased [*Battjes*, 1974]. Figure 25 shows the computed cross-shore variation of the time-averaged free surface elevation $\bar{\eta}$ above SWL after the establishment of periodicity. The setdown at the seaward boundary is extremely small for these cases with large values of d_t. Figure 25 and similar figures for the other cases indicate that the normalized setup $\bar{\eta}$ on the relatively steep slope is much greater than that on the gentle slope shown in Figure 11. This appears to be related to the thin layer of water remaining on the steep slope during wave downrush from the maximum wave runup elevation. Large values of the normalized setup $\bar{\eta}$ on a moderately steep beach were also measured by *Holman and Sallenger* [1985].

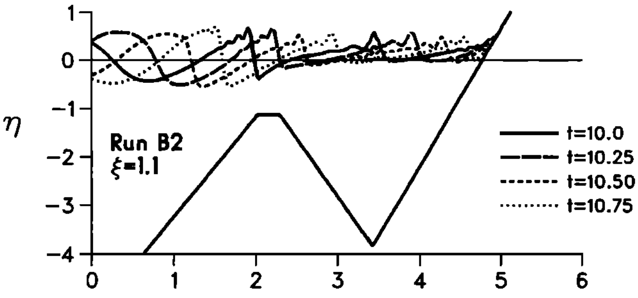

Fig. 35. Computed free surface variations over an idealized bar for run B2.

The computed reflection coefficients r for the seven cases listed in Table 1 are plotted in Figure 26 where the parameters ε_i and ε_r are defined as

$$\varepsilon_i = \frac{\pi}{K_s}\left(\frac{2\pi}{\tan\theta'}\right)^{1/2}\xi^{-2} \qquad \varepsilon_r = r\varepsilon_i \tag{25}$$

where K_s is the shoaling coefficient and $K_s = 1.11$ is assumed in Figure 26 on the basis of linear wave theory with $T' = 2.76$ s and $d_t' = 38$ cm. The solid lines given by $\varepsilon_r = \varepsilon_i$ for $\varepsilon_i < 1.6$ and $\varepsilon_r = 1.6$ for $\varepsilon_i \geq 1.6$ in Figure 26 were shown to follow the trend of scattered data points by *Guza and Bowen* [1976]. The numerical model underestimates the wave reflection coefficient considerably for these cases. The reflection coefficients for a 1:3 smooth slope computed by *Kobayashi and Watson* [1987] were in better agreement with the empirical formulas proposed by *Battjes* [1974] and *Seelig* [1983]. The difference may be related to the friction factor f' which has been taken to be 0.05 for small-scale smooth slopes on the basis of the limited calibration made for the 1:3 smooth slope by *Kobayashi and Watson* [1987]. In any case, the present numerical model is not really consistent with the experimental procedure adopted by *Guza and Bowen* [1976] for determining the reflection coefficient.

On the other hand, the computed swash oscillations on the 1:8.14 slope for the seven cases are summarized in Figure 27. The maximum, time-averaged, and minimum values of $Z_r(t)$ after the establishment of periodicity are denoted by R, $\bar{Z}_r$, and R_d, respectively. The values of R and R_d for $\delta_r' = 1$ and 10 mm as well as the value of $\bar{Z}_r$ for $\delta_r' = 1$ mm for each case are plotted as a function of ξ in Figure 27, where the value of ξ for each case is listed in Table 1. The computed values of $\bar{Z}_r$ for $1.34 \leq \xi \leq 4.24$ are of the order of unity and much greater than $\bar{Z}_r = 0.13$ for $\xi = 0.135$, as shown in Figures 4 and 11. The maximum runup R is less sensitive to the water depth δ_r' than the rundown R_d. Figure 27 also shows the empirical formulas $R = \xi$ for $0.1 < \xi < 2.3$ and $R_d = (\xi - 0.4\xi^2)$ for $0.3 < \xi < 1.9$, proposed by *Battjes* [1974]. The numerical model with $\delta_r' = 1$ mm and $f' = 0.05$ was found to slightly underestimate the maximum runup R on a 1:3 smooth slope, as compared to the empirical formula of *Ahrens and Martin* [1985], which is applicable for larger values of ξ as well [*Kobayashi and Watson*, 1987]. The computed values of R_d for

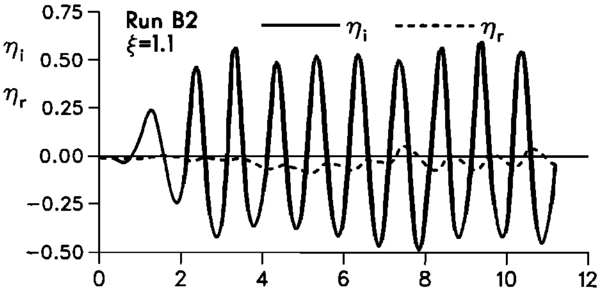

Fig. 37. Measured $\eta_i(t)$ and computed $\eta_r(t)$ for run B2.

$\delta_r' = 1$ mm fall on the dotted line for R_d shown in Figure 27. The normalized swash height may be defined as $(R - R_d)$. The computed swash heights for the seven cases are plotted in Figure 28 where ε_i is defined in (25) and ε_s is given by $\varepsilon_s = [\pi(R - R_d)/\xi^2]$. The solid curves given by $\varepsilon_s = \varepsilon_i$ for $\varepsilon_i < 1$, $\varepsilon_s = (\varepsilon_i)^{1/2}$ for $1 < \varepsilon_i < 9$, and $\varepsilon_s = 3$ for $\varepsilon_i > 9$ were shown to follow the trend of scattered data points by *Guza et al.* [1984]. The numerical model underestimates the value of ε_s for given ε_i, although the computed values of ε_s in Figure 28 are based on R for $\delta_r' = 1$ mm and R_d for $\delta_r' = 1$ cm shown in Figure 27 to increase the value of $(R - R_d)$ for each case. It is difficult to compare the numerical model to visually observed swash heights in light of the sensitivity of R_d and R to δ_r', as shown in Figures 23, 24, and 27.

In order to evaluate the numerical model in a more rigorous manner, small-scale tests were conducted in a wave tank which was 36 m long, 2.5 m wide, and 1.5 m deep. These tests were similar to the monochromatic wave tests conducted by *Kobayashi and Greenwald* [1986, 1988] for a 1:3 glued gravel slope and *Kobayashi and Watson* [1987] for a 1:3 plywood slope. The details of the present experiment were explained in the thesis of *Watson* [1988]. A piston-type wave maker controlled by a computer was used to generate specified incident wave trains in a burst, which were measured using a resistance wire wave gage with a wave-absorber beach in the tank. The bursting method eliminates the problem of waves reflected from the wave maker and is suited for the present time domain model. The water depth in the tank was kept constant and $d_t' = 40$ cm in these tests. The slope of given geometry installed in the tank was then exposed to the same incident wave trains.

Nine test runs were conducted as summarized in Table 2. A 1:8 plywood slope, which could be regarded as a smooth impermeable slope, was exposed to monochromatic waves with $T' = 1.2$, 2.0, and 3.2 s in runs S1, S2, and S3. In runs G1, G2, and G3 for the same 1:8 slope, transient-grouped waves were generated by superimposing two sinusoidal waves with equal heights and different periods. The wave period T' listed in Table 2 was the average of the two different periods, that is, 2.0 and 2.3 s for run G1, 2.6 and 3.4 s for run G2, and 2.8 and 3.6 s for run G3. In runs B1, B2, and B3 an idealized submerged bar installed at the toe of the 1:8 slope was subjected to monochromatic waves with $T' = 1.2$, 2.0, and 3.2 s, respectively. The crest of the bar was 45.5 cm wide and located at 8.5 cm below SWL. The seaward and landward slopes of the bar were given by $\cot \theta' = 11.1$ and -9.53, respectively, where the local angle of the slope has been defined in Figure 1. The landward edge of the bar and the 1:8 slope intersected at the depth of 29 cm below SWL. The representative wave height H' for each run was determined from the incident wave profile measured at the seaward boundary of the numerical model which was taken at the toe of the 1:8 slope for runs S1, S2, S3, G1, G2, and G3 and at the seaward edge of the bar for runs B1, B2, and B3. The height H' for each run listed in Table 2 was taken to be the average of the one-third highest waves in the measured incident wave train, although the variation of individual wave heights was not large for the monochromatic waves generated in a burst.

The dimensionless parameters d_t, ξ, and σ in Table 2 defined in (5), (6), and (7) were calculated using the values of T' and H' listed for each run together with $d_t' = 40$ cm and $\cot \theta' = 8$. The corresponding values of L and U_r were computed using cnoidal or Stokes second-order wave theory to indicate the representative values for each run. For the actual computation the measured incident wave profile normalized by H' for each run was used as input at the seaward boundary of the numerical model. This was also necessary because the wave maker was operated without regard to free second-harmonic waves [*Madsen*, 1971] and spurious low-frequency waves [*Kostense*, 1984]. The measurements made for each of the nine runs included the shoreline oscillation on the 1:8 slope and the free surface oscillation at the seaward boundary of the numerical model where the corresponding incident wave profile was measured with a wave-absorber beach in the tank. These measurements were synchronized and started at time $t' = 0$ slightly before the arrival of the specified incident wave train at the seaward boundary of the numerical model. The shoreline oscillation was measured using a capacitance-type wire gage placed along the centerline of the 1:8 slope and suspended between studs screwed into the plywood slope. The elevation of the gage above the plywood surface was approximately 1 cm, that is, $\delta_r' \simeq 1$ cm. This eliminated the uncertainty associated with visually observed swash oscillations.

Comparisons of the measured and computed results for the nine runs were presented in the thesis of *Watson* [1988], where $C_t = 0$ in (18) was assumed. The computed results presented in the following have employed $C_t = (16\ d_t)^{-1}$ to be consistent with the other computed results in this paper, although the differences between the computed results using $C_t = 0$ and $(16\ d_t)^{-1}$ have been found to be almost indistinguishable for these runs. Figure 29 shows the measured incident wave profile $\eta_i(t)$ and the computed variation of $\eta_r(t)$ at the toe of the 1:8 slope for run S2. The comparison between the measured and computed free surface oscillation $\eta_t(t)$ at the toe of the 1:8 slope is shown in Figure 30 where the computed oscillation $\eta_t(t)$ is the sum of $\eta_i(t)$ and $\eta_r(t)$ given in

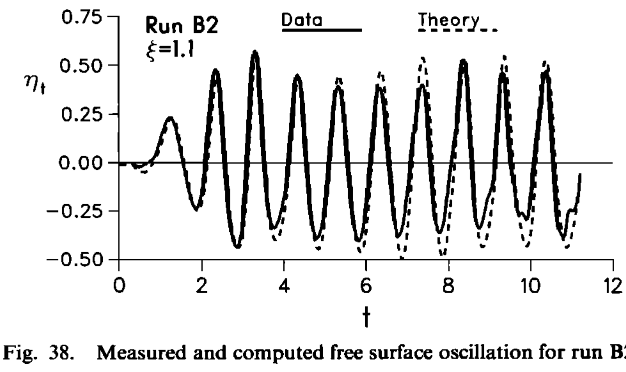

Fig. 38. Measured and computed free surface oscillation for run B2.

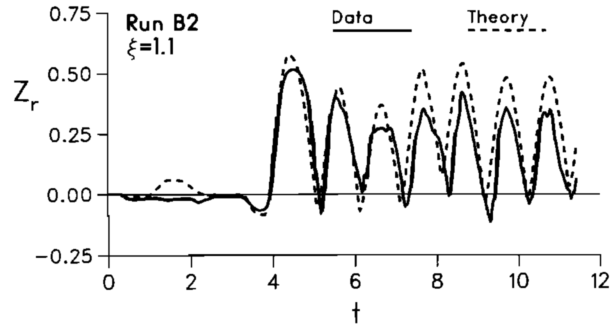

Fig. 39. Measured and computed shoreline oscillation for run B2.

Figure 29. Figure 31 shows the comparison between the measured and computed oscillation $Z_r(t)$ of the shoreline on the 1:8 slope where the instantaneous water depth is specified as $\delta_r' = 1$ cm. The degree of the agreement for runs S1 and S3 is very similar to that for run S2. The agreement for $\eta_t(t)$ appears to be good since the computed magnitude of $\eta_r(t)$ is relatively small for these cases. The previous comparison for a 1:3 slope indicated that the agreement for $\eta_t(t)$ would be poor if the numerical model could not predict the phase shift between the incident and large reflected wave profiles well [*Kobayashi and Greenwald*, 1988]. Figure 31 and similar figures for runs S1 and S3 indicate that the computed elevation Z_r tends to be somewhat lower than the measured elevation.

Likewise, Figures 32, 33, and 34 show the measured and computed oscillations for run G2. Comparing the grouped shoreline oscillation $Z_r(t)$ shown in Figure 34 with the grouped free surface oscillations $\eta_i(t)$ and $\eta_t(t)$ shown in Figures 32 and 33, the increase of the degree of grouping from the toe of the 1:8 slope to the shoreline is predicted fairly well by the numerical model. The compared results for runs G1 and G3 are similar to those for run G2, where the incident wave train for G1 is more grouped than that shown in Figure 32. These comparisons suggest that the numerical model may be applied to examine the interaction between incident wind waves and low-frequency motions on natural beaches.

On the other hand, the effects of an idealized bar on the shoreline oscillations on the 1:8 slope are examined in runs B1, B2, and B3. The computed free surface variations at t = 10, 10.25, 10.50, and 10.75 for run B2 are shown in Figure 35, which also depicts the idealized bar and the 1:8 slope. The seaward slope of the bar extends to $x = 0$, although it is not shown in Figure 35. The corresponding variations of the computed horizontal velocity u are shown in Figure 36. The effects of the bar on the wave transformation are apparent in these figures and similar figures for runs B1 and B3. The measured and computed oscillations for run B2 are shown in Figures 37, 38, and 39. The incident wave profiles for runs B1, B2, and B3 specified at the toe of the bar approximately correspond to those for runs S1, S2, and S3 specified at the toe of the 1:8 slope, respectively, as indicated in Table 2. The computed oscillation of $\eta_r(t)$ shown in Figure 37 is different from that shown in Figure 29 for run S2 probably because the presence of the bar modifies the wave reflection pattern. The agreement between the measured and computed free surface oscillation $\eta_t(t)$ shown in Figure 38 is not as good as that shown in Figure 30 for run S2. Comparing the measured and computed shoreline oscillation $Z_r(t)$ for run B2 shown in Figure 39 with that for run S2 shown in Figure 31, the numerical model is capable of predicting the reduction of the setup and swash oscillation caused by the presence of the bar. This conclusion also holds for runs B1 and B3 as compared to runs S1 and S3, respectively. These comparisons suggest that the numerical model may be applied not only to uniform slopes but also to beaches of arbitrary geometry, including a nearshore bar.

CONCLUSIONS

The numerical model developed previously for coastal structures has been modified to include the effect of the time-averaged current on the seaward boundary condition of the numerical model so as to improve the agreement between the measured and computed mean water levels on gentle slopes. The modified numerical model has been shown to yield fairly good agreement with small-scale test data on time-varying and time-averaged hydrodynamic quantities associated with monochromatic waves spilling on gentle slopes. The numerical model may be improved by matching its solution on the basis of the finite amplitude, shallow water equations with that based on the Boussinesq equations for a sloping bottom outside the breakpoint, since the equations used herein appear to be incapable of predicting wave shoaling over a long distance on the gentle slope because of the assumption of hydrostatic pressure. Moreover, the prediction of the undertow current in the surf zone may be improved by performing an additional analysis of the vertical variations of the time-averaged momentum and mass balances using the computed results of the present one-dimensional model as input to the analysis of the undertow. The analytical model for the undertow and bottom boundary layer flow proposed by *Svendsen et al.* [1987] required the measurements on the mean volume flux below the wave trough and the local force difference driving the undertow as input to their model.

As for steep slopes and beaches, the modification of the numerical model has been shown to result in negligible differences in the computed results as long as the seaward boundary of the numerical model is located in the water depth that is large relative to the incident wave height. The numerical model has also been shown to be in qualitative agreement with empirical formulas for the wave reflection coefficient and swash height for monochromatic waves plunging and surging on a relatively steep slope. In order to evaluate the capability of the numerical time domain model for predicting the reflected wave train and the shoreline oscillation on a relatively steep beach in a more rigorous and consistent manner, small-scale laboratory tests were conducted and measurements were analyzed in the time domain rather than the frequency domain. The numerical model has been shown to be capable of predicting the time-varying hydrodynamic quantities reasonably well even for incident transient grouped waves and an idealized beach profile with a nearshore bar. However, the friction factor f', which has been assumed to be constant for all the computations made in this paper, needs to be better established to reduce the uncertainties of the numerical model.

The comparisons made herein indicate that the numerical model may be applied to both gentle and steep beaches. As a result, the numerical model may be used to examine the interaction between incident wind waves and low-frequency motions in the cross-shore direction, since a specific beach with given geometry may be gentle and dissipative for wind waves but steep and reflective for low-frequency motions. Since the present time domain computation is not efficient for the incident irregular wave train of longer duration, it is desirable to develop a frequency domain model based on the finite amplitude, shallow water equations. This appears to be difficult since these equations are strongly nonlinear, unlike the Boussinesq equations for a sloping bottom which are weakly nonlinear [*Freilich and Guza*, 1984]. In addition, it is desirable to extend the numerical model to account for the alongshore variations of incident waves and beach topography, although computational efforts will increase considerably.

Acknowledgments. The authors would like to acknowledge the assistance of A. Wurjanto for computer program modifications. The first author would also like to thank I. A. Svendsen and R. T. Guza for discussions and reprints of their papers. This work is a result of research sponsored by NOAA Office of Sea Grant, Department of Commerce, under grant NA85AA-D-SG033 (project SG87 R/OE-3). The U.S. Government is authorized to produce and distribute reprints for government purposes, notwithstanding any copyright notation that may appear herein.

REFERENCES

Abbott, M. B., H. M. Petersen, and O. Skovgaard, On the numerical modelling of short waves in shallow water, *J. Hydraul. Res.*, *16*(3), 173–203, 1978.

Abbott, M. B., A. D. McCowan, and I. R. Warren, Accuracy of short-wave numerical models, *J. Hydraul. Eng. Am. Soc. Civ. Eng.*, *110*(10), 1287–1301, 1984.

Ahrens, J. P., and F. T. Martin, Wave runup formulas for smooth slopes, *J. Waterw. Port Coastal Ocean Eng. Am. Soc. Civ. Eng.*, *111*(1), 128–133, 1985.

Bailard, J. A., An energetics total load sediment transport model for a plan sloping beach, *J. Geophys. Res.*, *86*(C11), 10,938–10,954, 1981.

Battjes, J. A., Surf similarity, in *Proceedings of the 14th Coastal Engineering Conference*, pp. 466–480, American Society of Civil Engineers, New York, 1974.

Battjes, J. A., and M. J. F. Stive, Calibration and verification of a dissipation model for random breaking waves, *J. Geophys. Res.*, *90*(C5), 9159–9167, 1985.

Dean, R. G., and R. A. Dalrymple, *Water Wave Mechanics for Engineers and Scientists*, 353 pp., Prentice-Hall, Englewood Cliffs, N. J., 1984.

DeSilva, G. S., Wave transformation and cross-shore sediment transport in surf and swash zones, M. C. E. thesis, Univ. of Del., Newark, 1988.

Elgar, S., and R. T. Guza, Shoaling gravity waves: Comparisons between field observations, linear theory, and a nonlinear model, *J. Fluid Mech.*, *158*, 47–70, 1985*a*.

Elgar, S., and R. T. Guza, Observations of bispectra of shoaling surface gravity waves, *J. Fluid Mech.*, *161*, 425–448, 1985*b*.

Elgar, S., and R. T. Guza, Nonlinear model predictions of bispectra of shoaling surface gravity waves, *J. Fluid Mech.*, *167*, 1–18, 1986.

Flick, R. E., R. T. Guza, and D. L. Inman, Elevation and velocity measurements of laboratory shoaling waves, *J. Geophys. Res.*, *86*(C5), 4149–4160, 1981.

Freilich, M. H., and R. T. Guza, Nonlinear effects on shoaling surface gravity waves, *Philos. Trans. R. Soc. London, Ser. A*, *311*, 1–41, 1984.

Guza, R. T., and A. J. Bowen, Resonant interactions for waves breaking on a beach, in *Proceedings of the 15th Coastal Engineering Conference*, pp. 560–579, American Society of Civil Engineers, New York, 1976.

Guza, R. T., and E. B. Thornton, Swash oscillations on a natural beach, *J. Geophys. Res.*, *87*(C1), 483–491, 1982.

Guza, R. T., and E. B. Thornton, Velocity moments in nearshore, *J. Waterw. Port Coastal Ocean Eng. Am. Soc. Civ. Eng.*, *111*(2), 235–256, 1985*a*.

Guza, R. T., and E. B. Thornton, Observations of surf beat, *J. Geophys. Res.*, *90*(C2), 3161–3172, 1985*b*.

Guza, R. T., E. B. Thornton, and R. A. Holman, Swash on steep and shallow beaches, in *Proceedings of the 19th Coastal Engineering Conference*, pp. 708–723, American Society of Civil Engineers, New York, 1984.

Hansen, J. B., and I. A. Svendsen, A theoretical and experimental study of undertow, in *Proceedings of the 19th Coastal Engineering Conference*, pp. 2246–2262, American Society of Civil Engineers, New York, 1984.

Hibberd, S., and D. H. Peregrine, Surf and run-up on a beach: A uniform bore, *J. Fluid Mech.*, *95*(2), 323–345, 1979.

Holman, R. A., and A. H. Sallenger, Setup and swash on a natural beach, *J. Geophys. Res.*, *90*(C1), 945–953, 1985.

Huntley, D. A., R. T. Guza, and A. J. Bowen, A universal form for shoreline run-up spectra?, *J. Geophys. Res.*, *82*(18), 2577–2581, 1977.

Kobayashi, N., and J. H. Greenwald, Prediction of wave runup and riprap stability, in *Proceedings of the 20th Coastal Engineering Conference*, pp. 1958–1971, American Society of Civil Engineers, New York, 1986.

Kobayashi, N., and J. H. Greenwald, Waterline oscillation and riprap movement, *J. Waterw. Port Coastal Ocean Eng. Am. Soc. Civ. Eng.*, *114*(3), 281–296, 1988.

Kobayashi, N., and G. S. DeSilva, Motion of sediment particles in swash zone, in *Proceedings on Coastal Hydrodynamics*, pp. 715–730, American Society of Civil Engineers, New York, 1987.

Kobayashi, N., and K. D. Watson, Wave reflection and runup on smooth slopes, in *Proceedings on Coastal Hydrodynamics*, pp. 548–563, American Society of Civil Engineers, New York, 1987.

Kobayashi, N., A. K. Otta, and I. Roy, Wave reflection and runup on rough slopes, *J. Waterw. Port Coastal Ocean Eng. Am. Soc. Civ. Eng.*, *113*(3), 282–298, 1987.

Komar, P. D., and R. A. Holman, Coastal processes and the development of shoreline erosion, *Annu. Rev. Earth Planet. Sci.*, *14*, 237–265, 1986.

Kostense, J. K., Measurements of surf beat and set-down beneath wave groups, in *Proceedings of the 19th Coastal Engineering Conference*, pp. 724–740, American Society of Civil Engineers, New York, 1984.

Longuet-Higgins, M. S., and R. W. Stewart, Radiation stress and mass transport in gravity waves, with application to 'surf beats', *J. Fluid Mech.*, *13*, 481–504, 1962.

Madsen, O. S., On the generation of long waves, *J. Geophys. Res.*, *76*(36), 8672–8683, 1971.

Madsen, P. A., and I. R. Warren, Performance of a numerical short-wave model, *Coastal Eng.*, *8*, 73–93, 1984.

Moretti, G., Computation of flows with shocks, *Annu. Rev. Fluid Mech.*, *19*, 313–337, 1987.

New, A. L., P. McIver, and D. H. Peregrine, Computation of overturning waves, *J. Fluid Mech.*, *150*, 233–251, 1985.

Oltman-Shay, J., and R. T. Guza, Infragravity edge wave observations on two California beaches, *J. Phys. Oceanogr.*, *17*, 644–663, 1987.

Packwood, A. R., Surf and run-up on beaches, Ph.D. thesis, Univ. of Bristol, Bristol, U. K., 1980.

Peregrine, D. H., Long waves on a beach, *J. Fluid Mech.*, *27*, 815–827, 1967.

Peregrine, D. H., Breaking waves on beaches, *Annu. Rev. Fluid Mech.*, *15*, 149–178, 1983.

Seelig, W. N., Wave reflection from coastal structures, in *Proceedings of Coastal Structures '83*, pp. 961–973, American Society of Civil Engineers, New York, 1983.

Stive, M. J. F., Velocity and pressure field of spilling breakers, in *Proceedings of the 17th Coastal Engineering Conference*, pp. 547–566, American Society of Civil Engineers, New York, 1980.

Stive, M. J. F., A model for cross-shore sediment transport, in *Proceedings of the 20th Coastal Engineering Conference*, pp. 1550–1564, American Society of Civil Engineers, New York, 1986.

Stive, M. J. F., and H. G. Wind, A study of radiation stress and set-up in the nearshore region, *Coastal Eng.*, *6*, 1–25, 1982.

Suhayda, J. N., Standing waves on beaches, *J. Geophys. Res.*, *79*(21), 3065–3071, 1974.

Svendsen, I. A., Wave heights and set-up in a surf zone, *Coastal Eng.*, *8*, 303–329, 1984*a*.

Svendsen, I. A., Mass flux and undertow in a surf zone, *Coastal Eng.*, *8*, 347–365, 1984*b*.

Svendsen, I. A., and O. Brink-Kjaer, Shoaling of cnoidal waves, in *Proceedings of the 13th Coastal Engineering Conference*, pp. 365–383, American Society of Civil Engineers, New York, 1972.

Svendsen, I. A., and P. A. Madsen, A turbulent bore on a beach, *J. Fluid Mech.*, *148*, 73–96, 1984.

Svendsen, I. A., P. A. Madsen, and J. B. Hansen, Wave characteristics in the surf zone, in *Proceedings of the 16th Coastal Engineering Conference*, pp. 520–539, American Society of Civil Engineers, New York, 1978.

Svendsen, I. A., H. A. Schäffer, and J. B. Hansen, The interaction between the undertow and the boundary layer flow on a beach, *J. Geophys. Res.*, *92*(C11), 11,845–11,856, 1987.

Symonds, G., and A. J. Bowen, Interactions of nearshore bars with incoming wave groups, *J. Geophys. Res.*, *89*(C2), 1953–1959, 1984.

Symonds, G., D. A. Huntley, and A. J. Bowen, Two-dimensional surf beat: Long wave generation by a time-varying breakpoint, *J. Geophys. Res.*, *87*(C1), 492–498, 1982.

Watson, K. D., Waterline oscillations on smooth slopes and beaches, M. C. E. thesis, Univ. of Del., Newark, 1988.

N. Kobayashi and G. S. DeSilva, Ocean Engineering Program, Department of Civil Engineering, University of Delaware, Newark, DE 19716.

K. D. Watson, U.S. Army Corps of Engineers, Philadelphia District, Custom House, 2nd and Chestnut Street, Philadelphia, PA 19106.

(Received March 22, 1988;
accepted July 25, 1988.)